Absorption Spectrum of a Ru(II)−Aquo Complex in Vacuo − Resolving Individual Charge Transfer Transitions

ARTICLE *in* THE JOURNAL OF PHYSICAL CHEMISTRY A · NOVEMBER 2015

Impact Factor: 2.69 · DOI: 10.1021/acs.jpca.5b10488

2 AUTHORS:

Shuang Xu

University of Colorado Boulder

3 PUBLICATIONS **3** CITATIONS

SEE PROFILE

J Mathias Weber

University of Colorado Boulder

90 PUBLICATIONS **1,474** CITATIONS

SEE PROFILE

THE JOURNAL OF PHYSICAL CHEMISTRY A

Article

pubs.acs.org/JPCA

Absorption Spectrum of a Ru(II)-Aquo Complex in Vacuo: Resolving Individual Charge-Transfer Transitions

Shuang Xu[†,‡] and J. Mathias Weber*[,†,§]

[†]JILA, University of Colorado, 440 UCB, Boulder, Colorado 80309, United States

[‡]Department of Physics, University of Colorado, Boulder, Colorado 80309, United States

[§]Department of Chemistry and Biochemistry, University of Colorado, Boulder, Colorado 80309, United States

Supporting Information

ABSTRACT: Ruthenium(II) complexes are of great interest as homogeneous catalysts and as photosensitizers; however, their absorption spectra are typically very broad and offer only little insight into their electronic structure. We present the electronic spectrum of the aquo complex $[(trpy)(bipy)Ru^{II}-OH_2]^{2+}$ measured by photodissociation spectroscopy of mass-selected ions in vacuo (bipy = 2,2′-bipyridine and trpy = 2,2′:6′,2″-terpyridine). In the visible and near-UV, $[(trpy)(bipy)Ru^{II}-OH_2]^{2+}$ has several electronic bands that are not resolved in absorption spectra of this complex in solution but are partially resolved in vacuo. The experimental results are compared with results from time-dependent density functional theory calculations.

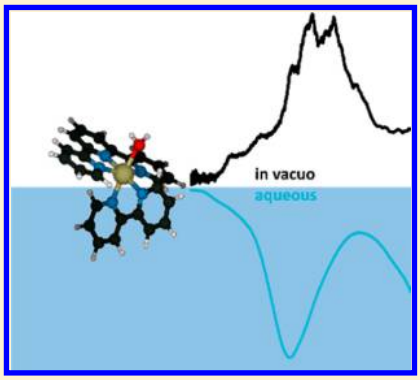

INTRODUCTION

One of the most promising avenues toward a sustainable energy economy, independent of the use of fossil fuels, is the conversion of CO_2 and water into chemical fuels. For this process to be economically viable, catalysts need to be developed for the various steps involved, but the molecular-level mechanisms in the catalytic generation of solar fuels are often poorly understood. At the current stage of research, it is important to investigate promising molecular catalysts and key intermediates in the proposed catalytic cycles in detail to connect molecular properties with catalyst performance, which can potentially guide catalyst design.

Investigating the fundamental processes and the detailed mechanisms involved in catalysis is a very challenging task. One of the main problems is the complexity of speciation in reactive solutions, making identification and study of catalysts and reaction intermediates difficult. In addition to speciation, solvation effects generally broaden the spectroscopic response of key species, often beyond the point at which different electronic bands can be distinguished, diminishing the level of detail available from UV/vis spectroscopy.

Spectroscopy of mass-selected ions from electrospray ionization (ESI) in vacuo offers an attractive experimental strategy to access the electronic structure of relevant species in more detail than is possible in condensed-phase experiments.[1−15] This is especially valuable to benchmark the reliability of various quantum chemical approaches.

Mononuclear Ru(II) complexes have received much attention as promising water oxidation catalysts in recent years.[16−22] These complexes strongly absorb in the visible spectral range, and their electronic structure is therefore important in solar fuel applications, whether intentionally (in photocatalysis) or as a side effect. One class of Ru(II) complexes that has been extensively studied is the aquo complex $[(bipy)(trpy)Ru-OH_2]^{2+}$ (**1**, see Figure 1) and its derivatives.[18−21,23,24]

The electronic absorption spectrum of this molecule in the visible and near-UV is the topic of the present work. The visible absorption spectrum of (**1**) in aqueous solution is characterized by a broad band in the visible region attributed to metal-to-ligand charge transfer (MLCT) transitions within the singlet manifold, with an onset at ca. 650 nm and a peak around 475 nm.[24] This feature is followed by very strong $\pi\pi^*$ transitions[24] at shorter wavelengths (below 350 nm).

Time-dependent density functional theory calculations by Jakubikova et al.[24] show several electronic singlet states giving rise to the broad visible absorption feature, but the different electronic bands are not resolved at all in UV/vis spectra of solutions at room temperature. While the time-dependent density functional theory (TDDFT) calculations previuosly mentioned qualitatively capture the envelope of the ^{1}MLCT band of (**1**) in solution, UV−vis spectroscopy in the condensed phase yields too little detail to allow identification of individual electronic bands, their intensity, or energy position. More detailed experimental data on the intrinsic electronic structure of the complex are needed to evaluate the validity of this

Received: October 26, 2015
Published: November 6, 2015

DOI: 10.1021/acs.jpca.5b10488
J. Phys. Chem. A 2015, 119, 11509−11513

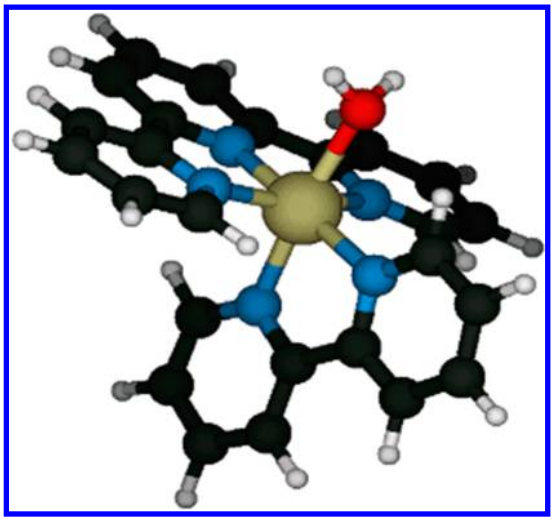

Figure 1. Ground-state structure of (**1**). Carbon atoms are shown in black, nitrogen in blue, ruthenium in gold, oxygen in red, and hydrogen in white.

approach. Here we report the photodissociation spectrum of (**1**) in vacuo in the visible and near-UV.

METHODS

Experimental Section. The target complex (**1**) was synthesized as described in the literature.[16−22] Working with mass-selected ions of (**1**) allowed working with raw product solutions (i.e., without purification). The experimental setup belongs to a class of similar apparatus used by several groups[25−32] and has recently been described elsewhere.[33] In brief, experiments were performed using a custom-built photodissociation spectrometer that combines an ESI source, an ion trap, a tandem time-of-flight mass spectrometer (TOF-MS), and a tunable pulsed laser source (see Figure 2). Solution

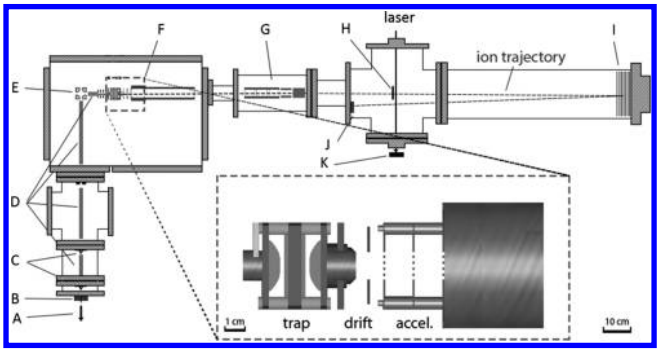

Figure 2. Schematic overview of the experimental setup. (A) ESI needle; (B) desolvation capillary; (C) skimmers; (D) octupole ion guides; (E) quadrupole bender; (F) ion trap and acceleration stage (see insert for details); (G) ion optics; (H) mass gate; (I) reflectron; (J) microchannel plate detector; and (K) pyroelectric joulemeter.

of (**1**) in a 4:1 (by volume) ethanol−water mixture was electrosprayed using N_2 as nebulizing gas. After passing a desolvation capillary, ions were focused through a skimmer into a series of three octupole ion guides in successive differential pumping stages. In the final pumping stage, ions were steered with a combination of a quadrupole bender, another short octupole guide, and a series of tube lenses into a 3D Paul trap, where they were thermalized in collisions with He buffer gas (at room temperature) and accumulated for ca. 50 ms.

After the accumulation phase, ions were injected into a TOF-MS. At the space focus of the TOF-MS, ions were mass-selected using a pulsed mass gate and irradiated with the output of a pulsed beta barium borate-based optical parametric converter system pumped by the third harmonic of a Nd:YAG laser. The signal wavelength (710−405 nm) was used directly or was sum-frequency-mixed with the Nd:YAG fundamental (1064 nm) for conversion to shorter wavelengths. After irradiation, ions traveled for ca. 15−20 μs before entering a two-stage reflectron for fragment mass analysis. A dual microchannel plate detector was used for ion detection. Mass selection, irradiation, and fragment ion analysis were carried out under conditions where collisions with background gas can be neglected (pressures were in the range of 10^{-7} mbar). The TOF-MS was operated at 20 Hz repetition rate, while the laser was operated at 10 Hz to distinguish photofragment and background signal. The photodissociation spectrum was recorded by monitoring the intensity of fragment ions corresponding to the loss of the water ligand as a function of photon energy, corrected for photon fluence. Several scans were averaged and measured on different days to ensure reproducibility.

Computational. We used density functional theory[34] employing B3LYP[35,36] and PBE0[37] functionals and def2-TZVP basis sets for all atoms as implemented in the Turbomole suite of programs[38,39] to calculate the ground-state structure of (**1**) without symmetry restrictions. Electronic excitation spectra were calculated using TDDFT[40−42] with the same functionals and basis sets.

RESULTS AND DISCUSSION

Figure 3 shows the electronic photodissociation action spectrum of (**1**) obtained by photodissociation of the mass

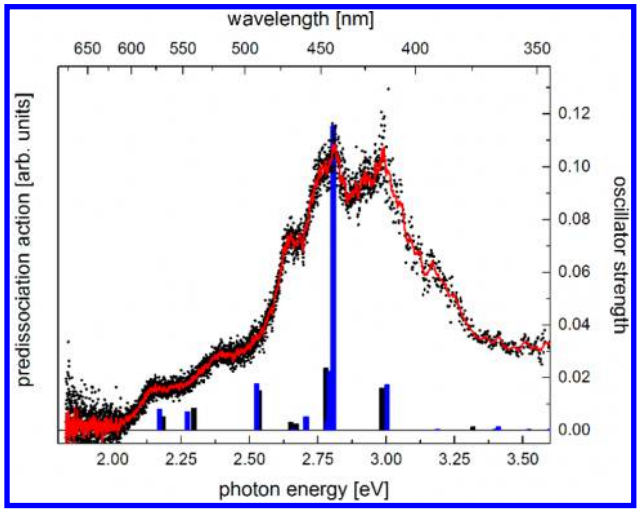

Figure 3. Photodissociation action spectrum of (**1**), monitoring the loss of the water ligand from 1.8 to 3.6 eV. The data points are raw data, and the full line is a 10-point gliding average. The spectrum is composed of four overlapping traces through different tuning ranges of the laser. Columns represent TDDFT calculations performed with the PBE0 functional (blue, shifted by −0.3 eV) and with the B3LYP functional (black, shifted by −0.15 eV). The full spectrum including UV photon energies up to 4.8 eV is shown in the Supporting Information (Figure S1).

DOI: 10.1021/acs.jpca.5b10488
J. Phys. Chem. A 2015, 119, 11509−11513

Table 1. Electronic Excited States up to 3.6 eV[a]

excited state	E [eV]/f [10^{-3}] B3LYP	E [eV]/f [10^{-3}] PBE0	E_{exp} [eV] ± 0.03 eV	character of leading orbitals
S_1	2.19/5.26	2.17/8.19	2.16	d → trpy
S_2	2.30/8.50	2.27/7.04	2.40	d → trpy
S_3	2.54/11.5	2.53/17.8	2.65	d → trpy
S_4	2.65/3.14	2.66/0.54		d → bipy
S_5	2.67/2.51	2.71/5.24		d → trpy
S_6	2.77/0.049	2.78/3.37		d → bipy
S_7	2.78/23.7	2.79/22.6		d → trpy
S_8	2.81/109	2.81/115	2.81	d → trpy
S_9	2.98/16.1	3.00/17.3	3.00	d → bipy
S_{10}	3.10/0.091	3.19/0.045		d → water
S_{11}	3.32/1.34	3.41/1.29		d → water
S_{12}	3.40/0.37	3.51/0.25		d → water
S_{13}	3.52/0.29	3.60/0.49		d → bipy/trpy

[a]The second and third columns show excitation energies in electronvolts and oscillator strengths for results from B3LYP and PBE0 calculations, respectively. B3LYP energies were shifted by −0.15 eV from the raw calculated energies, while PBE0 energies were shifted by −0.30 eV. The fourth column shows tentative assignments of experimental features where applicable. The last column describes the main character of the leading transition orbitals for each transition. All transitions are MLCT transitions within the singlet manifold. Additional information is listed in Table S1 and Figure S2 (see Supporting Information).

selected complex in vacuo at room temperature. The spectrum has an onset at 2.05 eV (605 nm) and shows several partially resolved features with an increasing band shape that peaks at 2.81 eV (443 nm), followed by a second peak of roughly the same intensity at 3.00 eV. We use the average energy of these two intense features to determine the solvatochromic red shift in aqueous solution as 0.3 eV, somewhat greater than in $Ru(bipy)_3^{2+}$.[43,44] It is important to note that not all excited states have the same solvatochromic shift. For instance, the onset of the spectrum (2.06 eV in vacuo) is red-shifted by 0.15 eV in aqueous solution.[24]

For molecules the size of (**1**), TDDFT represents a good compromise between quality and cost because methods at higher levels are often computationally too expensive. While long-range charge-transfer transitions are problematic,[45,46] typical MLCT transitions can often be treated reasonably well using hybrid functionals.[47,48] We compare our experimental results with TDDFT calculations using PBE0 and B3LYP functionals (see Table 1). Both calculations are in rough agreement with the envelope of the experimental spectrum (see Figure 3), but the dominant peaks are shifted by 0.3 (PBE0) and 0.15 eV (B3LYP) to higher energies compared with the experiment. Shifting the calculated transitions to the red by these amounts yields very similar "stick" spectra for the two functionals, and some of the calculated transitions correspond very well to experimentally observed features, in particular, the lowest excited state and the most intense feature; however, we caution that the assignments shown in Table 1 are based on the calculated sequence of the five most intense electronic transitions and should be treated as tentative.

The lowest energy transition ($S_0 \rightarrow S_1$) mainly involves the highest occupied molecular orbital (HOMO, metal-d-character) and the lowest unoccupied molecular orbital (LUMO, mostly localized on trpy). In general, the nine lowest energy transitions can be characterized as ^{1}MLCT transitions from different metal d orbitals to the organic ligands (mostly trpy, sometimes also bipy). At higher energies (>3 eV), weaker ^{1}MLCT transitions involving the water ligand are predicted as well. Contour plots of the leading orbitals are shown in the Supporting Information (Figure S2). Our computational results are in very good agreement with those of Jakubikova et al.[24]

For the photodissociation spectrum to be directly comparable to the photoabsorption spectrum, the photodissociation quantum yield must be unity or at least independent of wavelength throughout the spectral region of interest. In the absence of solvent and collisions (which is the case in the present experiment), the only way to lose energy upon excitation is via photon emission or fragmentation. In other words, the photoemission quantum yield should be negligible and the fragmentation quantum yield should be largely independent of photon energy in the range where the molecules absorb. Both of these conditions will be discussed in the following paragraphs.

Metal organic Ru(II) complexes often relax very quickly by intersystem crossing into the lowest ^{3}MLCT state[49] and subsequently phosphoresce. However, (**1**) is only weakly emissive at room temperature.[22,24] In fact, photon emission from (**1**) has been found to be so weak that it competes in intensity with CH stretching Raman bands from the ligands.[24] We therefore assume that it can be neglected and that nonradiative transitions to the electronic ground state will be by far the main de-excitation pathway.

Neglecting photon emission, the energy deposited in the molecule upon photon absorption produces a vibrationally hot ion via internal conversion, which leads to unimolecular decay, typically on a sub-microsecond to microsecond time scale. Such unimolecular decay typically proceeds via the dissociation channel with the lowest threshold energy, which in (**1**) is the loss of the water ligand (calculated threshold energy 1.1 eV = 106 kJ/mol). The remaining question is whether fragmentation will occur with close to unit quantum yield during the observation time of our experiment. If this condition were not met, we would observe a spectrum with photofragment yields that are suppressed at lower photon energies, distorting the peak shape (kinetic shift). We have tested for kinetic shift effects by acquiring spectra with ion beam kinetic energies of 4.0 and 2.6 keV, corresponding to observation times of ca. 16 and 20 μs under otherwise identical conditions. If the unimolecular decay time upon photon absorption resulted in a kinetic shift for these observation times, we would expect a clear difference between the two spectra, but the two data sets have identical shapes within the statistical error of the data (see

DOI: 10.1021/acs.jpca.5b10488
J. Phys. Chem. A 2015, 119, 11509−11513

Supporting Information, Figure S3). Because we can neglect photon emission and can rule out kinetic shift effects on the peak shape, we conclude that the photodissociation spectrum is equivalent to the photoabsorption spectrum. While molecules of this size store substantial amounts of vibrational energy (at room temperature ~0.75 eV in excess of zero point energy according to our calculations), the addition of ≥1.8 eV by photon absorption seems to be sufficient to overcome kinetic shift effects.

A point of interest in the context of excited-state dynamics is that the lowest energy ^{1}MLCT band, appearing in the spectrum as a shoulder at 2.15 eV (577 nm), is far below the two most intense peaks in the envelope of the spectrum at 2.91 eV (426 nm). An important consequence is that excitation into the apparent peak of the broad ^{1}MLCT band will not bring the molecule to the S_1 state but to some higher lying excited state. This may have profound consequences for the excited-state dynamics of the system prepared in this fashion. In addition, it should be realized that ultrafast experiments, which necessarily have a broad bandwidth, will very likely excite a superposition of several electronic bands. Finally, the spatial distribution of electron density in different excited states can be very different as well (see Figure S3). These issues may complicate the interpretation of ultrafast experiments on (**1**) and related systems.

Some of the width of the observed bands is likely due to the temperature of the ions, which we assume to be the temperature of the ion trap (i.e., room temperature), causing the appearance of hot bands and leading to spectral congestion; however, lifetime broadening may also contribute to some of the observed width, as intersystem crossing lifetimes in most Ru(II) complexes are usually very short (<100 fs).[49] Finally, the ^{1}MLCT transitions are likely to lead to changes in geometry, particularly for the metal−ligand bond lengths. Therefore, spectral congestion due to the unresolved Franck−Condon envelope of each electronic band is also a likely source of the observed widths.

CONCLUSIONS

We show that the electronic spectrum of mass-selected ions of (**1**) obtained in vacuo exhibits pronounced structure. This allows for the first time a quantitative comparison of experimental and computational spectroscopic results for this complex. Computational data from TDDFT overestimate the observed band positions by 0.15 (B3LYP) to 0.3 (PBE0) eV but represent the relative energies of assigned resolved states rather well (within ca. 0.1 eV). The set of spectroscopic features in the visible spectral region can be identified as a set of superimposed, partially resolved electronic bands in the manifold of ^{1}MLCT transitions, which mainly involve the trpy ligand. The envelope of the observed bands peaks at 2.91 eV (426 nm), corresponding to a solvatochromic shift of −0.3 eV in aqueous solution. The lowest electronic band is at 2.15 eV, quite far removed from the peak of the envelope. This may complicate the interpretation of ultrafast experiments on related systems.

ASSOCIATED CONTENT

Supporting Information

The Supporting Information is available free of charge on the ACS Publications website at DOI: 10.1021/acs.jpca.5b10488.

The electronic photodissociation spectrum up to 5 eV, a comparison of the photodissociation spectrum of (**1**) in the visible region obtained at two different ion beam energies, orbitals involved in electronic transitions (B3LYP), TDDFT excited states up to 3.6 eV, and coordinates of (**1**) obtained using B3LYP/def2-TZVP. (PDF)

AUTHOR INFORMATION

Corresponding Author

*E-mail: weberjm@jila.colorado.edu.

Notes

The authors declare no competing financial interest.

ACKNOWLEDGMENTS

We gratefully acknowledge support from the National Science Foundation under Grant CHE-1361814.

REFERENCES

(1) Spence, T. G.; Burns, T. D.; Guckenberger, G. B.; Posey, L. A. Wavelength-Dependent Photodissociation of $[Fe(bpy)_3 \cdot (CH_3OH)_n]^{2+}$ Clusters, n = 2−6, Triggered by Excitation of the Metal-to-Ligand Charge-Transfer Transition. *J. Phys. Chem. A* **1997**, *101*, 1081−1092.

(2) Spence, T. G.; Trotter, B. T.; Burns, T. D.; Posey, L. A. Metal-to-Ligand Charge Transfer in the Gas-Phase Cluster Limit. *J. Phys. Chem. A* **1998**, *102*, 6101−6106.

(3) Calvo, M. R.; Andersen, J. U.; Hvelplund, P.; Nielsen, S. B.; Pedersen, U. V.; Rangama, J.; Tomita, S.; Forster, J. S. Photophysics of Protoporphyrin Ions in Vacuo: Triplet-State Lifetimes and Quantum Yields. *J. Chem. Phys.* **2004**, *120*, 5067−5072.

(4) Nielsen, S. B.; Andersen, L. H. Properties of Microsolvated Ions: From the Microenvironment of Chromophore and Alkali Metal Ions in Proteins to Negative Ions in Water Clusters. *Biophys. Chem.* **2006**, *124*, 229−237.

(5) Friedrich, J.; Gilb, S.; Ehrler, O. T.; Behrendt, A.; Kappes, M. M. Electronic Photodissociation Spectroscopy of Isolated IrX_6^{2-} (X = Cl,Br). *J. Chem. Phys.* **2002**, *117*, 2635−2644.

(6) Kordel, M.; Schooss, D.; Gilb, S.; Blom, M. N.; Hampe, O.; Kappes, M. M. Photodissociation of Trapped Metastable Multiply Charged Anions: A Routine Electronic Spectroscopy of Isolated Large Molecules? *J. Phys. Chem. A* **2004**, *108*, 4830−4837.

(7) Greisch, J. F.; Harding, M. E.; Kordel, M.; Klopper, W.; Kappes, M. M.; Schooss, D. Intrinsic Fluorescence Properties of Rhodamine Cations in Gas-Phase: Triplet Lifetimes and Dispersed Fluorescence Spectra. *Phys. Chem. Chem. Phys.* **2013**, *15*, 8162−8170.

(8) Wang, X. B.; Yang, X.; Wang, L. S. Probing Solution-Phase Species and Chemistry in the Gas Phase. *Int. Rev. Phys. Chem.* **2002**, *21*, 473−498.

(9) Yang, X.; Wang, X. B.; Vorpagel, E. R.; Wang, L. S. Direct Experimental Observation of the Low Ionization Potentials of Guanine in Free Oligonucleotides by Using Photoelectron Spectroscopy. *Proc. Natl. Acad. Sci. U. S. A.* **2004**, *101*, 17588−17592.

(10) Waters, T.; Wang, X. B.; Wang, L. S. Electrospray Ionization Photoelectron Spectroscopy: Probing the Electronic Structure of Inorganic Metal Complexes in the Gas-Phase. *Coord. Chem. Rev.* **2007**, *251*, 474−491.

(11) Dean, J. C.; Walsh, P. S.; Biswas, B.; Ramachandran, P. V.; Zwier, T. S. Single-Conformation UV and IR Spectroscopy of Model G-Type Lignin Dilignols: The Beta-O-4 and Beta-Beta Linkages. *Chem. Sci.* **2014**, *5*, 1940−1955.

(12) Dean, J. C.; Burke, N. L.; Hopkins, J. R.; Redwine, J. G.; Ramachandran, P. V.; McLuckey, S. A.; Zwier, T. S. UV Photofragmentation and IR Spectroscopy of Cold, G-Type Beta-O-4 and Beta-Beta Dilignol-Alkali Metal Complexes: Structure and Linkage-Dependent Photofragmentation. *J. Phys. Chem. A* **2015**, *119*, 1917−1932.

DOI: 10.1021/acs.jpca.5b10488
J. Phys. Chem. A 2015, 119, 11509−11513

(13) Houmøller, J.; Kaufman, S. H.; Støchkel, K.; Tribedi, L.; Nielsen, S. B.; Weber, J. M. On the Photoabsorption by Permanganate Ions in Vacuo and the Role of a Single Water Molecule. New Experimental Benchmarks for Electronic Structure Theory. *ChemPhysChem* **2013**, *14*, 1133−1137.
(14) Kaufman, S. H.; Weber, J. M.; Pernpointner, M. Electronic Structure and UV Spectrum of Hexachloroplatinate Dianions in Vacuo. *J. Chem. Phys.* **2013**, *139*, 194310−1−194310−10.
(15) Kaufman, S. H.; Weber, J. M. Photodissociation Spectroscopy of the Anionic Copper Nitrate Association Complex $Cu(NO_3)_3^-$. *J. Phys. Chem. A* **2014**, *118*, 9687−9691.
(16) Zong, R.; Thummel, R. P. A New Family of Ru Complexes for Water Oxidation. *J. Am. Chem. Soc.* **2005**, *127*, 12802−12803.
(17) Wasylenko, D. J.; Palmer, R. D.; Berlinguette, C. P. Homogeneous Water Oxidation Catalysts Containing a Single Metal Site. *Chem. Commun.* **2013**, *49*, 218−227.
(18) Concepcion, J. J.; Tsai, M.-K.; Muckerman, J. T.; Meyer, T. J. Mechanism of Water Oxidation by Single-Site Ruthenium Complex Catalysts. *J. Am. Chem. Soc.* **2010**, *132*, 1545−1557.
(19) Wasylenko, D. J.; Ganesamoorthy, C.; Koivisto, B. D.; Henderson, M. A.; Berlinguette, C. P. Insight into Water Oxidation by Mononuclear Polypyridyl Ru Catalysts. *Inorg. Chem.* **2010**, *49*, 2202−2209.
(20) Concepcion, J. J.; Jurss, J. W.; Norris, M. R.; Chen, Z.; Templeton, J. L.; Meyer, T. J. Catalytic Water Oxidation by Single-Site Ruthenium Catalysts. *Inorg. Chem.* **2010**, *49*, 1277−1279.
(21) Concepcion, J. J.; Jurss, J. W.; Brennaman, M. K.; Hoertz, P. G.; Patrocinio, A. O. T.; Iha, N. Y. M.; Templeton, J. L.; Meyer, T. J. Making Oxygen with Ruthenium Complexes. *Acc. Chem. Res.* **2009**, *42*, 1954−1965.
(22) Hewitt, J. T.; Concepcion, J. J.; Damrauer, N. H. Inverse Kinetic Isotope Effect in the Excited-State Relaxation of a Ru(Ii)-Aquo Complex: Revealing the Impact of Hydrogen-Bond Dynamics on Nonradiative Decay. *J. Am. Chem. Soc.* **2013**, *135*, 12500−12503.
(23) Weinberg, D. R.; Gagliardi, C. J.; Hull, J. F.; Murphy, C. F.; Kent, C. A.; Westlake, B. C.; Paul, A.; Ess, D. H.; McCafferty, D. G.; Meyer, T. J. Proton-Coupled Electron Transfer. *Chem. Rev.* **2012**, *112*, 4016−4093.
(24) Jakubikova, E.; Chen, W. Z.; Dattelbaum, D. M.; Rein, F. N.; Rocha, R. C.; Martin, R. L.; Batista, E. R. Electronic Structure and Spectroscopy of $[Ru(Tpy)_2]^{2+}$, $[Ru(Tpy)\ (Bpy)(H_2o)]^{2+}$, and [Ru-(Tpy) (Bpy)Cl]$^+$. *Inorg. Chem.* **2009**, *48*, 10720−10725.
(25) Wang, L. S.; Ding, C. F.; Wang, X. B.; Barlow, S. E. Photodetachment Photoelectron Spectroscopy of Multiply Charged Anions Using Electrospray Ionization. *Rev. Sci. Instrum.* **1999**, *70*, 1957−1966.
(26) Asmis, K. R.; Brümmer, M.; Kaposta, C.; Santambrogio, G.; von Helden, G.; Meijer, G.; Rademann, K.; Wöste, L. Mass-Selected Infrared Photodissociation Spectroscopy of $V_4O_{10}^+$. *Phys. Chem. Chem. Phys.* **2002**, *4*, 1101−1104.
(27) Rizzo, T. R.; Stearns, J. A.; Boyarkin, O. V. Spectroscopic Studies of Cold, Gas-Phase Biomolecular Ions. *Int. Rev. Phys. Chem.* **2009**, *28*, 481−515.
(28) Kamrath, M. Z.; Relph, R. A.; Guasco, T. L.; Leavitt, C. M.; Johnson, M. A. Vibrational Predissociation Spectroscopy of the H_2-Tagged Mono- and Dicarboxylate Anions of Dodecanedioic Acid. *Int. J. Mass Spectrom.* **2011**, *300*, 91−98.
(29) Hock, C.; Kim, J. B.; Weichman, M. L.; Yacovitch, T. I.; Neumark, D. M. Slow Photoelectron Velocity-Map Imaging Spectroscopy of Cold Negative Ions. *J. Chem. Phys.* **2012**, *137*, 244201.
(30) Duffy, E. M.; Marsh, B. M.; Garand, E. Probing the Hydrogen-Bonded Water Network at the Active Site of a Water Oxidation Catalyst: $Ru(bpy)\ (tpy)(H_2O)^{2+}\cdot(H_2O)_{0-4}$. *J. Phys. Chem. A* **2015**, *119*, 6326−6332.
(31) Wolk, A. B.; Leavitt, C. M.; Garand, E.; Johnson, M. A. Cryogenic Ion Chemistry and Spectroscopy. *Acc. Chem. Res.* **2014**, *47*, 202−210.
(32) Redwine, J. G.; Davis, Z. A.; Burke, N. L.; Oglesbee, R. A.; McLuckey, S. A.; Zwier, T. S. A Novel Ion Trap Based Tandem Mass Spectrometer for the Spectroscopic Study of Cold Gas Phase Polyatomic Ions. *Int. J. Mass Spectrom.* **2013**, *348*, 9−14.
(33) Xu, S.; Gozem, S.; Krylov, A. I.; Christopher, C. R.; Weber, J. M. Ligand Influence on the Electronic Spectra of Monocationic Copper-Bipyridine Complexes. *Phys. Chem. Chem. Phys.* **2015**, DOI: 10.1039/C5CP05063D.
(34) Parr, R. G.; Yang, W. *Density-Functional Theory of Atoms and Molecules*; Oxford University Press: New York, 1989.
(35) Becke, A. D. Density-Functional Exchange-Energy Approximation with Correct Asymptotic-Behavior. *Phys. Rev. A: At., Mol., Opt. Phys.* **1988**, *38*, 3098−3100.
(36) Lee, C. T.; Yang, W. T.; Parr, R. G. Development of the Colle-Salvetti Correlation-Energy Formula into a Functional of the Electron-Density. *Phys. Rev. B: Condens. Matter Mater. Phys.* **1988**, *37*, 785−789.
(37) Perdew, J. P.; Burke, K.; Ernzerhof, M. Generalized Gradient Approximation Made Simple. *Phys. Rev. Lett.* **1996**, *77*, 3865−3868.
(38) Weigend, F.; Ahlrichs, R. Balanced Basis Sets of Split Valence, Triple Zeta Valence and Quadruple Zeta Valence Quality for H to Rn: Design and Assessment of Accuracy. *Phys. Chem. Chem. Phys.* **2005**, *7*, 3297−3305.
(39) Weigend, F.; Häser, M.; Patzelt, H.; Ahlrichs, R. Ri-Mp2: Optimized Auxiliary Basis Sets and Demonstration of Efficiency. *Chem. Phys. Lett.* **1998**, *294*, 143−152.
(40) Bauernschmitt, R.; Ahlrichs, R. Treatment of Electronic Excitations within the Adiabatic Approximation of Time Dependent Density Functional Theory. *Chem. Phys. Lett.* **1996**, *256*, 454−464.
(41) Bauernschmitt, R.; Häser, M.; Treutler, O.; Ahlrichs, R. Calculation of Excitation Energies within Time-Dependent Density Functional Theory Using Auxiliary Basis Set Expansions. *Chem. Phys. Lett.* **1997**, *264*, 573−578.
(42) Furche, F. On the Density Matrix Based Approach to Time-Dependent Density Functional Response Theory. *J. Chem. Phys.* **2001**, *114*, 5982−5992.
(43) Kirketerp, M. B. S.; Nielsen, S. B. Absorption Spectrum of Isolated Tris(2,2′-Bipyridine)Ruthenium(II) Dications in Vacuo. *Int. J. Mass Spectrom.* **2010**, *297*, 63−66.
(44) Stockett, M. H.; Nielsen, S. B. Communication: Does a Single CH_3CN Molecule Attached to $Ru(bipy)_3^{2+}$ Affect Its Absorption Spectrum? *J. Chem. Phys.* **2015**, *142*, 171102.
(45) Dreuw, A.; Head-Gordon, M. Single-Reference Ab Initio Methods for the Calculation of Excited States of Large Molecules. *Chem. Rev.* **2005**, *105*, 4009−4037.
(46) Tozer, D. J.; Amos, R. D.; Handy, N. C.; Roos, B. O.; Serrano-Andres, L. Does Density Functional Theory Contribute to the Understanding of Excited States of Unsaturated Organic Compounds? *Mol. Phys.* **1999**, *97*, 859−868.
(47) Adamo, C.; Scuseria, G. E.; Barone, V. Accurate Excitation Energies from Time-Dependent Density Functional Theory: Assessing the PBE0Model. *J. Chem. Phys.* **1999**, *111*, 2889−2899.
(48) Adamo, C.; Barone, V. A TDDFT Study of the Electronic Spectrum of S-Tetrazine in the Gas-Phase and in Aqueous Solution. *Chem. Phys. Lett.* **2000**, *330*, 152−160.
(49) Yoon, S.; Kukura, P.; Stuart, C. M.; Mathies, R. A. Direct Observation of the Ultrafast Intersystem Crossing in Tris(2,2′-Bipyridine) Ruthenium(II) Using Femtosecond Stimulated Raman Spectroscopy. *Mol. Phys.* **2006**, *104*, 1275−1282.

DOI: 10.1021/acs.jpca.5b10488
J. Phys. Chem. A 2015, 119, 11509−11513